

# We are IntechOpen, the world's leading publisher of Open Access books Built by scientists, for scientists

6,900

Open access books available

186,000

International authors and editors

200M

Downloads

Our authors are among the

154

Countries delivered to

TOP 1%

most cited scientists

12.2%

Contributors from top 500 universities



WEB OF SCIENCE™

Selection of our books indexed in the Book Citation Index  
in Web of Science™ Core Collection (BKCI)

Interested in publishing with us?  
Contact [book.department@intechopen.com](mailto:book.department@intechopen.com)

Numbers displayed above are based on latest data collected.  
For more information visit [www.intechopen.com](http://www.intechopen.com)



# Multilevel Information Fusion: A Mixed Fuzzy Logic/Geometrical Approach with Applications in Brain Image Processing

Julien Montagner<sup>1</sup> and Vincent Barra<sup>2</sup>

<sup>1</sup> LaTIM, INSERM U650; Institut TELECOM, TELECOM Bretagne; UEB,

<sup>2</sup>LIMOS, UMR CNRS 6158 Université Blaise Pascal  
France

## 1. Introduction

### 1.1 A definition of information and image fusion

The principle of information fusion is widely used in image-based processes where the data are acquired from several sources, e.g. in the fields of remote sensing (Lennon et al., 2000), satellite (Wald, 2002) or biomedical imaging (Barra & Boire, 2001a). L. Wald defined the fusion operation as “a formal framework in which are expressed the means and tools for the alliance of data originating from different sources”. According to the same author, the aim of a fusion process is to improve the quality of the available information, where the notion of quality depends on the application context. I. Bloch et al. give a more specific definition of fusion: “data fusion consists in combining several pieces of information issued from different sources about the same phenomenon, in order to take a better decision on this phenomenon” (Bloch & Maître, 1997). In accordance with this statement, the fusion of image data is viewed as the joined use of heterogeneous images for decision aid.

The first and most obvious difference between these definitions (and the numerous others proposed in the literature) lies in the aim of the fusion process. That is, the goal to reach is here either to improve the information provided by the different sources, each of them considered as being imperfect (Dubois & Prade, 1994), or to take a decision about the observed scene. The first objective may be viewed as a qualitative improvement (reducing information imperfections), while in the second case the aim is to reduce the doubt about the validity of the decision by increasing the amount of available information. This last case may thus also be viewed as a quantitative improvement of the information.

Whatever the definition for the fusion process, data stemming from one source are generally used to compensate for a lack of information or as a medium for complementary features about the physical object or phenomenon studied. In this chapter, image fusion will refer to a computer-based process aiming at extracting knowledge from an image set, which was obviously not visible in the original images. This new information may consist in either image data (visual result) (Aguilar & New, 2002; Montagner et al., 2005a), numerical indexes (Wang et al., 1998; Montagner et al., 2005b), or even subsets of image regions (image segmentation in e.g. binary sets) (Bloch et al., 2003).

Source: Sensor and Data Fusion, Book edited by: Dr. ir. Nada Milisavljević,  
ISBN 978-3-902613-52-3, pp. 490, February 2009, I-Tech, Vienna, Austria

### 1.2 Relevance of information fusion in computer-based diagnosis-aid processes

In the general field of medical imaging, with a special interest here for the study of the human brain, the collection of various data coming from anatomical and functional imagery is becoming very common for the study of a given pathology. The treatment of these data is performed by a physicist, who analyses and aggregates them according to his knowledge. The aim is to provide a better medical decision, to propose a prognosis, or to assist physicians in a surgical intervention. This approach may clearly be modeled and automated by means of an information fusion process, with the interest of providing accurate numerical information to the physicist.

The sensitive nature of the brain makes imaging to be a major investigation tool (rather than a surgical approach), and one can find many medical examples and interests for such an automatic process. Morphological aspects of the human brain are mainly studied using magnetic resonance imaging (MRI). An MR image is a 3D data volume that gives information on structural composition of the organ (distribution of tissues, fine spatial resolution). It can be obtained using a wide range of parameters, so that the resulting images provide sufficient contrasts between the different structures to be located (tissue interfaces, tumors, etc.). The brain may also be studied from a functional point of view, using two major functional modalities: PET and SPECT (positron/single photon emission tomography). The images are obtained by injecting or inhaling a radioactive tracer that preferentially characterized a physiologic (e.g. glucose metabolism) or a biologic (e.g. blood flow) process, and then measuring the resulting particle emission. Both PET and SPECT provide 3D datasets reconstructed from these planar projections (Hudson & Larkin, 1994). Such images have a poor spatial resolution and are not informative on what they are not supposed to represent. Figure 1 shows examples of anatomical and functional images of a same brain.

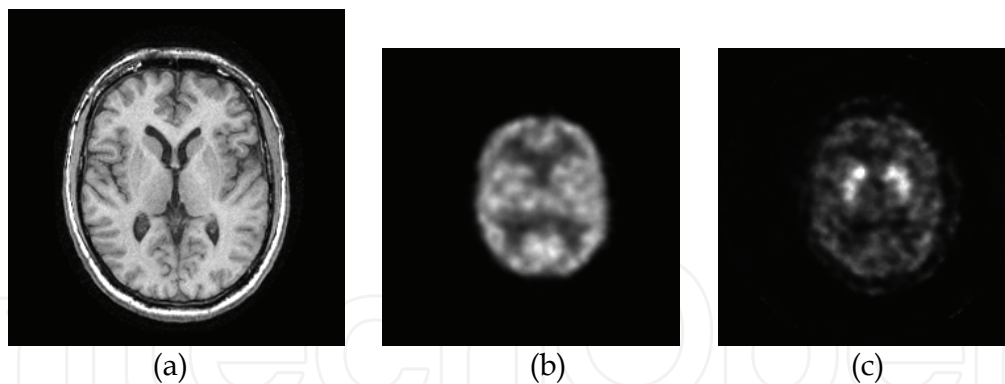


Fig. 1. Three views of a same brain: anatomical (a. MR image) and functional (b. and c. SPECT images respectively showing the blood perfusion and dopamine receptors density)

The main interest of a fusion between information stemming from both MR and such functional images is to supply anatomical information for the accurate detection of pathologic areas characterized in functional imaging by physiological abnormalities (Barra & Boire, 2000b, Barra & Boire, 2001a ). Clinical implications are various and numerous, from the detection of functional abnormalities in the study of dementia (Julin & al., 1997) to the precise location of activity sites in neurotransmission SPECT imaging, or the accurate quantification of monoamine transmitters density. Several examples of the fusion scheme we propose will be detailed at the end of this chapter. From a more clinical standpoint, these applications of multisource medical brain imaging can be explained as follows:

- brain tissue segmentation can be carried out as an accurate mean of quantifying the volume of brain matters in diseases such as Alzheimer's dementia, epilepsy, or hydrocephalus, for purpose of diagnosis, treatment, and general understanding;
- accurate segmentation of subcortical brain structures is a fundamental issue in several applications like the assessment of structural brain abnormalities, the study of abnormal entities (e.g. carcinoma), the mapping of functional activation onto human anatomy, the study of brain disorders (e.g. schizophrenia) or computer-assisted neurosurgery;
- effects of Parkinson's disease and Parkinsonian syndromes on striatal structures are commonly characterized by mean of functional imaging (Catafau, 2001). However, an early detection of these effects remains inaccessible to the single visual examination of SPECT (or even PET) images. A quantification process can provide objective numerical indexes in relation with the pathology severity, but it highly depends on the difficult location of regions of interest (ROIs). A fusion with a morphological image of the same brain may represent a suitable solution to this critical segmentation problem;
- new diagnosis elements may also be obtained by the synthesis of an image holding both functional and anatomical information. An advanced fusion strategy (not limited to a color channel combination) allows the physicist to select image features to be displayed, to avoid spatial covering or frequency mixing that would hinder a good perception of the diagnostic information (e.g. hypoperfused gray matter for patients suffering from probable Alzheimer's disease (Colin & Boire, 1999)).

### 1.3 Managing characteristics and structure of heterogeneous image information

When considering the fusion process, input images intensities are often not directly compatible, owing to their numerical nature (numerical type, value range, etc.) and, above all, their physical meaning. Aggregating the information held by two corresponding pixels thus implies to model this information in a common formalism. Handling heterogeneous data also occurs when considering information stemming from different sensors, but of different types (e.g. signal and image sensor, expert knowledge and image sensor). Here again, a common theoretical formalism is needed to embed these data, and the choice of this framework is guided by the nature of available information.

As stated above, medical information acquired from automated sensors, and especially medical images, holds an imperfect information in a sense commonly admitted in the field of information fusion: data are often subject to many uncertainties (e.g. which tissue class(es) associated with a given image intensity range?), possibly due to both inaccuracies (e.g. quantization of image intensities, single value standing for large spatial regions) and/or some inherent ambiguities (e.g. several possible reasons/classes).

SPECT images are a relevant example of these uncertainties. In addition to the mandatory corrections of scattering and other quality-loss phenomena during the tomographic reconstruction (i.e. attenuation, depth-dependent resolution, etc.) (Soret et al., 2003), computer-based diagnosis processes have to face the problem of low spatial resolution intrinsically linked with SPECT images (PET images having a higher resolution, but being more expensive). Consequently, the 3D reconstruction process builds quite large-size voxels, and generates partial volume effects (PVE). Even after PVE correction (Boussion et al., 2006), the image information is therefore the object of some imprecision that makes it impossible to accurately define the boundaries of anatomical structures of interest. Furthermore, the functional information held by tomoscintigraphic images is intrinsically not well fitted to

such a task, because of its possible double meaning: if a low image intensity theoretically follows a low fixation rate of the tracer, it nevertheless remains difficult to determine from the image alone whether this level is associated with an out-of-structure site, or to an abnormal functional activity within structure boundaries (Fig. 2).

The three most common approaches used to represent and manage heterogeneous information in that context are the well known probability theory, the belief functions theory (Shafer, 1976), and the possibilistic logic based on the fuzzy sets formalism (Zadeh, 1978 ; Dubois & Prade, 2004).

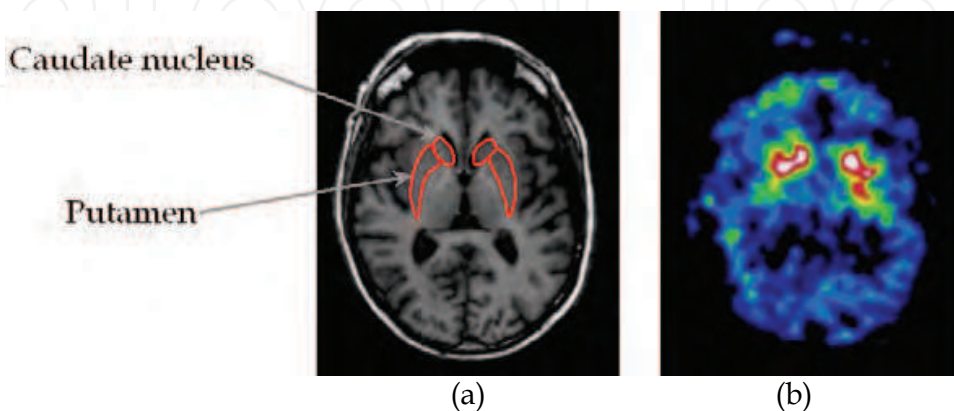


Fig. 2. Co-registered MR (a. showing striatal structures) and neurotransmission SPECT images (b); Outlines of caudate nuclei are roughly defined on (b), whereas boundaries of putamens disappear with the loss of dopamine receptors

Digital images stemming from acquisition processes cited in 1.2 are composed of discrete sets of numerical values (2D/3D arrays of image intensities), standing for given features of the physical phenomenon measured. A pixel (or voxel in 3D) from one of these images is viewed here as the region of the real space in which the associated value has been quantified. Both the numerical aspects and the spatial distribution of image intensities have therefore to be managed in the fusion process, each of these features being of equal relevance in the definition of image information. If the questions of information modeling and aggregation of numerical information using fuzzy sets or other uncertainty models have been widely studied, the problem of spatial matching of data sets to fuse is often considered of secondary importance.

In the case where all images have the same size and spatial resolution, a fusion process can sometimes be directly performed by aggregating information stemming from image numerical values (Bloch, 1996) associated with a unique pixel (with the same index in image arrays). This is only possible if acquisitions have been made from in the same geometrical referential, and if the object of interest is represented with the same size in each image. Since this configuration rarely occurs (because of practical acquisition constraints such as sensor size or spatial and temporal resolutions), most numerical values in a given image don't have direct spatial correspondence with intensities from other data sets (Fig. 3).

In order to manage both geometrical relations (only affine relations are addressed here because of the nature of organs we are interested in) and the difference in spatial resolution between images, most methods process the image information in a multiscale context. Such processes are either based on frequency analysis of data, e.g. managing all image information on a common wavelet base (Pajares & De La Cruz, 2004), or on a "resolution hierarchy" obtained by iterative degradation of original images (Matsopoulos et al., 1994).

The problem is often reduced to the trivial fusion case presented above by a simple registration of image data in a common geometrical base, including an interpolation of numerical data. But the choice of an interpolation method relies on strong assumptions (e.g. linear variation of the measured phenomenon in the real space) that on the one hand simplify the fusion, but also introduce some unwanted imprecision in the data that may hinder an accurate quantification of brain activity in MRI/SPECT fusion. In this case, authors only commonly align the MR image on the SPECT image in order to preserve data to quantify (Soret et al., 2003 ; Rousset et al., 1998). But this method dramatically decreases the anatomical precision.

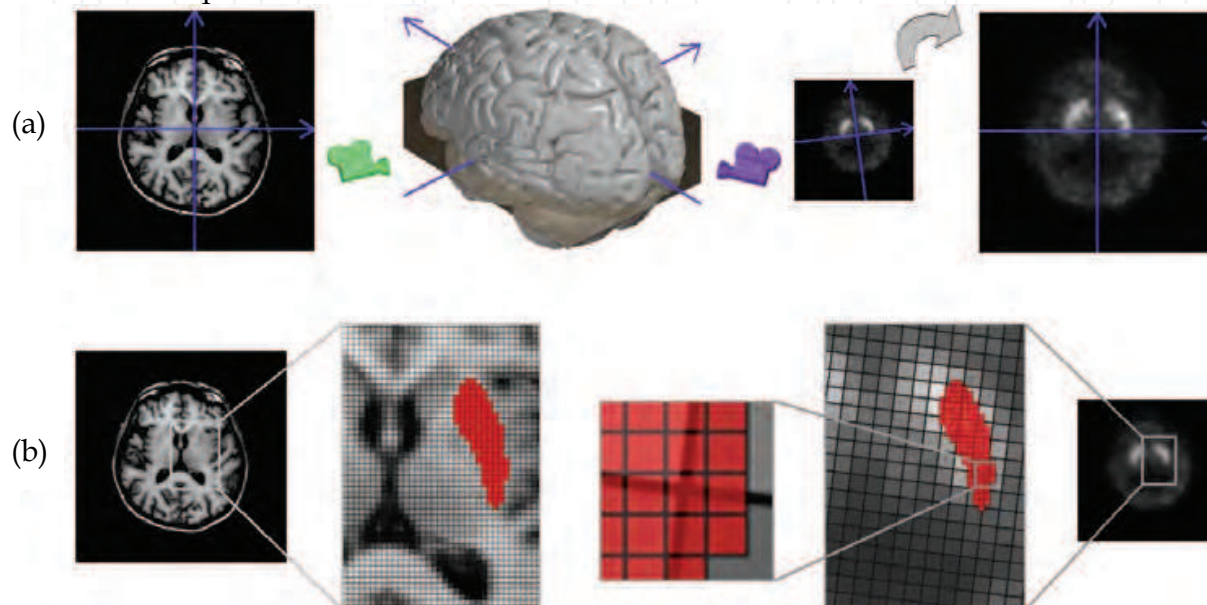


Fig. 3. a. A slice from MR (left) and SPECT (right - original and registered) images of the same brain; b. Consequences of co-registration on voxels from original images through the example of an anatomical structure (putamens)

#### 1.4 A fusion framework for medical images

This chapter describes an information fusion scheme devoted to 2D/3D medical images. Both the different stages of this process and the global architecture were designed to answer practical problems and give assistance for diagnosis using medical image processing and information fusion. This work is typically related to the fusion of different kind of medical images (in which numerical intensities express different physical phenomena), with different spatial orientation and resolution. In the following, the method is presented through examples of brain images processing and illustrated in the case of two input images, although it can be applied to both a more general fusion problem and to other organs. Details of the method are given under the assumption that input images are 3D datasets (collections of voxels), but the extension to the 2D images case is trivial. Most of the illustrations are given in 2D for visual convenience.

The fusion process we propose here is guided by the intrinsic nature of images, viewed as digital information embedded with a given geometrical structure. This multilevel fusion scheme is designed to manage the possibly different spatial distributions of image data apart from other heterogeneity sources, in order to preserve the accuracy of initial data through the whole process. The fuzzy formalism is used as a theoretical framework to

represent image data, and possibly other kind of information (e.g. expert knowledge). The management of image geometrical features is based on principles and algorithms stemming from the field of discrete geometry to preserve the accuracy of original data to fuse (avoiding early interpolation).

The first part of this chapter is centered on the presentation of methodological aspects of this work. Section 2 introduces the general structure of the generic fusion scheme. Sections 3 and 4 respectively focus on the theoretical background for the fuzzy modeling/fusion of image numerical data, and geometric principles and algorithms used for the management of the spatial structure of input images.

Depending on both the nature of the information to fuse and the objective of the fusion, the tools defined by this fusion scheme may be used in several scenarios. For example, fusing two images with different spatial resolution will highly take benefit from the management of image geometrical features, while the fusion of an image with symbolic information (i.e. with no particular spatial structure) will only require a single-level fusion based on fuzzy modeling. Moreover, this fusion scheme is versatile enough to allow multistage fusion too: during the modeling stage, the information representation may also consists in a first complete fusion process.

The second part of this chapter presents three practical examples of brain image fusion relying on the proposed scheme in the case of three different scenarios. Section 5.1 illustrates an example of a 1 level/1 stage fusion scenario aiming at the refinement of brain tissue segmentation from multispectral MR images. The second fusion level (management of image spatial features) is first illustrated in section 5.2 (1 stage only), with the synthesis of an unique image from multimodal information sources. Finally, section 5.3 illustrates the 2 levels/2 stages fusion process, by means of a functional quantification of the brain activity from SPECT images, using an MR image to locate anatomical structures of interest. The segmentation of such anatomical structures is driven by expert information in a first MRI/symbolic information fusion.

## 2. A theoretical framework for the fusion process

### 2.1 General fusion scheme

This fusion architecture is an improvement of an existing fusion process, that was designed making use of fuzzy logic (Barra & Boire, 2001a). Input images were supposed to be initially aligned, and this first registration stage was followed by three fusion steps:

1. Information modeling step: datasets were first represented in a common theoretical formalism, in order to compensate for the heterogeneous nature of the information provided by the images. The choice of using fuzzy logic is explained in section 3.1, and details on the modeling itself are given in sections 3.2.
2. Aggregation step: information models were injected into a fitted fusion operator, designed to either produce a new information expressed under the same formalism, or to emphasize information buried into original images (section 3.3).
3. Decision step: the information produced by the previous step was taken back to the relevant numerical domain or to the decision context in which the fusion process is involved, possibly resulting in a final formalism conversion. Moreover, this step came possibly out to a crisp information model ( $\alpha$ -cut, thresholding, etc.), once the amount of information aggregated during the fusion process was sufficient to take a decision.

As stated above, the major problem for e.g. activity quantification purpose using morphological and functional images is the initial registration stage that introduces some additional uncertainties about the information to measure. The generic fusion scheme proposed in this chapter is designed to be possibly used both for classical fusion tasks, i.e. to answer fusion problems that were previously coped thanks to the fusion process presented above, and to preserve as long as possible the accuracy of initial data for a use in more complex fusion problems based for example on multiresolution data.

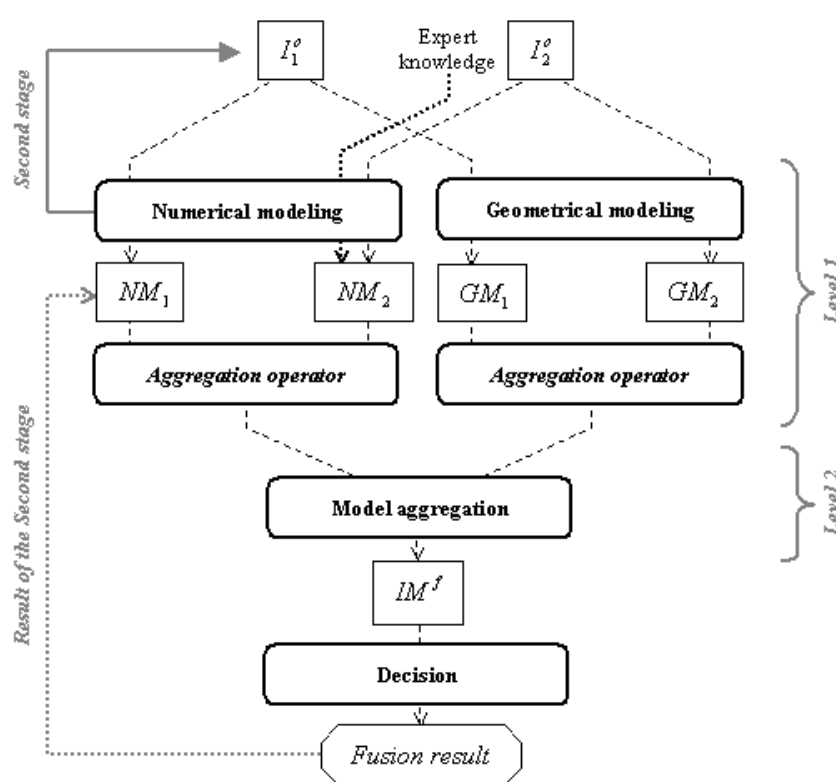


Fig. 4. A synoptic diagram of the fusion process designed in this chapter. This process is illustrated in the case of two input images  $I_i^o, i \in \{1,2\}$ , each being represented by both a numerical model  $NM_i$  and a geometrical model  $GM_i$ ; The final aggregation stage provides a fused information model  $IM^f$  that leads to a decision in the sense given above (point 3)

For this last purpose, all information sets cannot always be modeled using the same formalism, or can even not get modified at the modeling stage (e.g. binary masks of ROIs vs. original SPECT data). This methodological aspect is the first particularity of the fusion process we now propose: the modeling step is extended to the use of compatible theoretical frameworks, which have together a physical meaning, instead of strictly equivalent formalisms. The problem to be solved here is more particularly to give both information stemming from the modeling stage a spatial coherence.

To do so while preserving the accuracy of initial information, we choose to delay the management of this spatial correspondence as far as possible in the fusion process. The solution we propose consists in managing the image spatial structure apart from image numerical intensities. For each input image, these two sets of characteristics are modeled separately, leading to running (partially) two independent fusion processes in parallel.

Fusion operators are designed to aggregate information models in each domain. These operators are finally combined to provide the final aggregation function (Fig. 4), transforming information represented by intensities and structural information models together into the final fusion result.

## 2.2 Definitions and relations with classical information fusion processes

The modeling, aggregation and decision stages presented above are commonly accepted as a structure for fusion-based processes (Wald, 2002). The estimation of information models, considered as an additional task by some authors, is for us fully included in the modeling stage (as shown in 3.2). Each branch of the improved version of the process (Fig. 4) follows the same classical scheme, until aggregation operators are designed to achieve a global fusion between corresponding voxels from input images, represented in the corresponding formalism (i.e. voxel to voxel/geometrical matching of image structures at the voxel level, as described in section 4).

Dasarathy proposed three levels of fusion (Dasarathy, 1997), corresponding to three abstraction levels for representing information: data fusion (values directly provided by the sensors), feature fusion (information derived from previous data) and decision fusion (information expressing hypothesis to be confirmed). The process depicted on Figure 4 is composed of two fusion levels, the first one being performed separately on the two image features sets. This first level clearly occurs at the feature level, since input images are first modeled in each domain, and no decision is moreover taken until both aggregation models are combined. This last step can be associated to an additional fusion level considered by some authors: model fusion, aiming at combining pieces of information that represent a method or process.

A distinction is usually made between two kinds of information as an input of the fusion process: numerical information vs. symbolic information. The architecture of the fusion process described in this chapter allows the description of two other categories of information extracted from input images: structural information of digital images, managed through the right path of the schematic description of the process (Fig. 4), and numerical models of image semantic information (left path). This last category is obviously not independent from a classical description of input information, since it may refer to numerical representation (fuzzy logic) of both image numerical intensities and symbolic information transcribed in the same geometrical referential as image data. Because of the theoretical frames chosen to represent structural information and the previous group of information type, we may also refer to these domains as respectively the geometrical (or spatial) model and the numerical model.

## 2.3 The different scenarios of fusion

Depending on both the spatial referential in which are expressed the information to fuse and the aim of the fusion, applications based on the scheme described here may use only one or both processing paths illustrated on Figure 4. Considering the left branch alone (no geometrical information to manage), the model aggregation level is then avoided, and the combination operator at level 1 may thus achieve a single-level feature-based aggregation, directly providing  $IM^f$  (Fig. 7.a and 11.b).

The multistage aspect of the fusion architecture refers to the ability to achieve building the image numerical model as a complete iteration of the fusion process (Fig. 11). Image

intensities are injected as inputs for the sub-fusion process. Consequently, this fusion stage is carried out based on numerical models only, but may also involve external sources such as expert knowledge (symbolic information) (Fig. 11.b). The result of the sub-fusion stage is then used as a model of image numerical intensities in the first stage process.

### 3. Numerical information modeling and related aggregation operators

#### 3.1 Possibilistic logic as a theoretical framework

Data we will have to manage are quite imprecise and uncertain, due for example to partial volume effects or noise. We, thus chose to model these data with a theory managing uncertainty and imprecision, and we particularly focused on possibilistic logic. Possibilistic logic was introduced by Zadeh in (Zadeh, 1978) in order to simultaneously represent and manage imprecise and uncertain knowledge. In fuzzy set theory, a fuzzy measure is a representation of the uncertainty, giving for each subset  $Y$  of the universe of discourse  $X$  a coefficient in  $[0,1]$  assessing the degree of certitude for the realization of the event  $Y$ . In possibilistic logic, this fuzzy measure is modeled as a measure of possibility  $\Pi$  satisfying  $\Pi(\emptyset)=0, \Pi(X)=1$  and  $\Pi \cup_i Y_i = \sup_i \Pi(Y_i)$ . An event  $Y$  is fully possible if  $\Pi(Y)=1$ , and impossible if  $\Pi(Y)=0$ . Zadeh showed that  $\Pi$  could completely be defined from the assessment of the certitude on each singleton of  $X$ . Such a definition relies on the definition of a distribution of possibility  $\pi$ , satisfying  $\sup_{x \in X} \pi(x)=1$ . Fuzzy and crisp sets can then be represented by distributions of possibility, from the definition of their characteristic function.

We choose the possibilistic logic as the common theoretical frame for the representation of the available data. More precisely, we model all the information using distributions of possibility, and equivalently we represent this information using fuzzy sets.

#### 3.2 Information modeling: from image data to semantic knowledge

We consider in the following two types of information to be represented by numerical models: the information extracted from images, we call the numerical information, which mainly consists in tissue characterization (morphological images) or activity distribution (functional images), and the symbolic or semantic information modeling the linguistic data that may be provided by an expert.

- *Numerical information:* numerical information is directly extracted from images, and is modeled as distributions of possibility either representing brain tissues, (cerebrospinal fluid (CSF), white matter (WM) and gray matter (GM) distributions in morphological images), or distribution of the functional activity. These distributions are computed using a possibilistic clustering algorithm (Krishnapuram & Keller, 1993) on particular feature vectors representing voxels (Barra & Boire, 2000b). If each voxel  $1 \leq j \leq N$  is described by a  $p$ -dimensional feature vector  $x_j$ , the possibilistic clustering algorithm is an iterative algorithm that searches for  $C$  compact clusters gathering in  $X = \{x_j\}$  the  $x_j$ 's by computing both a fuzzy partition matrix  $U = (u_{i,j})$ ,  $1 \leq i \leq C$ ;  $1 \leq j \leq N$ ,  $u_{ij} = \pi_i(j)$  being the membership degree of  $x_j$  to class  $i$ , and unknown cluster centers  $B = (b_i), 1 \leq i \leq C$ . The algorithm uses iterative optimizations to find the minimum of a constrained objective function

$$J(B, U, X) = \sum \sum u_{ij}^m d^2(x_j, b_i) + \sum \eta_i \sum (1 - u_{ij})^m \quad (1)$$

subject to  $u_{ij} \in [0, 1]$ ,  $\sum u_{ij} < N$ ,  $\max_i u_{ij} > 0$  and  $\eta_i$  being the intra-class mean fuzzy distance as proposed in (Krishnapuram & Keller, 1996). Parameter  $m$  controls the degree of fuzziness of  $U$ , and is chosen equal to 2 in the following.  $d$  is the Euclidean distance in  $R^p$ .

- *Semantic information*: symbolic information was given by clinicians and experts and consisted in topological and morphological information. These fuzzy propositions might typically be modeled in the possibilistic logic frame. We already propose a theoretical framework to model approximate distance and direction information as fuzzy sets and we refer the reader to (Barra & Boire, 2001b) for a detailed description of the modeling process.

### 3.3 Aggregating the information: definition of fusion operators

Fuzzy sets and the possibilistic logic both offer a wide range of combination operators and a flexible way to choose them. (Bloch, 1996) proposed a classification of these operators with respect to their behavior (in terms of conjunctive, disjunctive or compromise), the possible control of this behavior, their properties and their decisiveness, which proved to be useful for several applications in image processing.

Generally speaking, a fusion operator aggregates  $N_i$  distributions of possibility  $\pi^i$  into a fused distribution  $\pi$ , using a fusion operator  $F : \pi = F(\pi^1, \dots, \pi^N)$ . The definition of  $F$ , its mathematical properties and its behaviour with respect to the agreement and the conflict between the  $\pi^i$  are driven by the application. Some examples of such fusion operators are given in the application section.

## 4. Spatial information modeling and fusion using discrete geometry

The core of the proposed method is a geometrical model representing the spatial structure of input images at the voxel level, and allowing the fusion of the corresponding features considering geometrical relation between images. This model has been chosen considering the fusion process backward, from model aggregation to the modeling stage. The central point was to give the spatial information a final form that was compatible with the final information stemming from the fusion of numerical models, making it possible to merge fusion operators which produced them.

### 4.1 The redistribution principle: getting coefficients from spatial relations

In the case where a two-levels fusion is performed, the final aggregation stage we propose to carry out is called "redistribution" (i.e. redistribution of the numerical information held by image voxels). The information provided by the geometrical aggregation operator aims at representing spatial relations between images by simple sets of numerical values (spatial coefficients). These values, thus consistent with image numerical models, are thereafter used during the final aggregation stage, as weighting factors in the assignment of data from one image or information model to another one (usually from a low-resolution one to a high-

resolution one in a multiresolution problem), in order to compensate for the difference of spatial referential (orientation, resolution, etc.).

If we again consider the two images case, let  $\rho$  be a spatial coefficient locally modeling spatial relations between both images. Since the elementary part of a 3D digital image is the voxel,  $\rho = \rho(v_1, v_2)$  models the basic spatial relation between a voxel  $v_1$  from image  $I_1$  and a voxel  $v_2$  from image  $I_2$ . Note that in the following,  $v$  and  $V$  will stand for  $v_1$  and  $v_2$  for typographic convenience. This notation is moreover justified since images  $I_1$  and  $I_2$ , in the case where they have to be geometrically registered, often have different spatial resolution that implies voxels with different sizes. Voxel  $v$  thus denotes the spatial element with the highest resolution/the smallest voxel size, and  $V$  the element with the largest size.

Spatial coefficients have to express spatial relations between both images, in order to combine information really stemming from the same spatial location. Image numerical intensities are obtained by integrating the measured phenomenon in regions of the real space corresponding to image voxels. To study the spatial distribution of image intensities and spatial relations linking an image to another one, the model thus simply consists in representing the influence region of each numerical value during the measurement, i.e. modeling image voxels themselves. Modeling the whole image thus boils down to define a tiling of the image space by these voxel models.

For the sake of simplicity, only the case of cubic voxels is addressed here (an hexagonal model is for instance a better representation of a spherical influence area, but leads to much more time-consuming algorithms). Discrete geometrical tools used in the following have been chosen under this assumption. The digital nature of image information has also guided the choice of the processing operator used to obtain spatial coefficients from the geometrical models. The question of studying spatial relations between two voxel lattices is indeed very close to the classical discrete coordinates changing problem (Reveilles, 2001). Discrete and computational geometry provide efficient tools to answer such a problem.

The extension of the tiling created by image voxels to the whole space may be considered as a discrete coordinate system. Therefore, the problem of spatially matching a given image with another one is intrinsically linked with the question of accurately expressing, in a target basis  $B_2$ , discontinuous information from a basis  $B_1$ ,  $B_1 \neq B_2$ . A solution was proposed in (Reveilles, 2001) with a suitable formalism for 3D image fusion. When images have close or equal spatial resolutions, the ratio between edge length of  $v$  and  $V$  is not sufficient to disregard the committed error when rounding to integers the results of classical basis change formulas (Fig. 5). In this case, one shall determine the volume of the geometrical intersection between unit elements of the grids and use this value in an interpolation step. Hence, this last processing stage finally appears to be compulsory, but guided by all the available image spatial information.

#### 4.2 Geometrical modeling and fusion operators based on computational geometry

Both the difference in spatial resolution and the spatial misalignment of corresponding structures in images have to be managed during the modeling. When considering two images  $I_1$  and  $I_2$ , these spatial features make information from  $I_1$  and  $I_2$  to be expressed in two different geometrical spaces, which have to be linked through the geometrical model.

The geometrical transform resulting from the usual registration step is not applied to the data (and in particular data are not interpolated), but we use the corresponding mathematical function to generate the geometrical model. Both images are modeled as

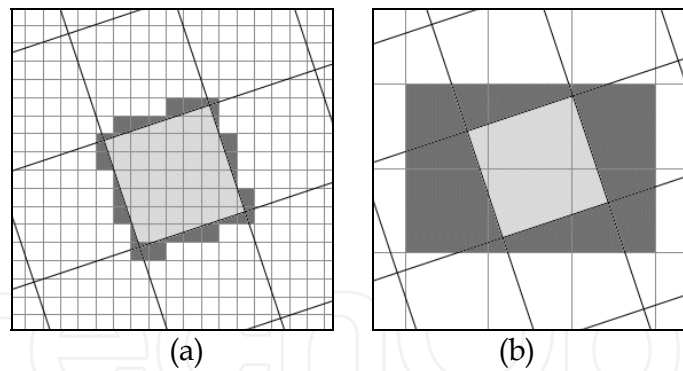


Fig. 5. Illustration of the discrete coordinates changing problem in 2D (a. different grid sizes, b. grids with quite similar pixels). Basis change formulas associate part of pixels in light gray to the right pixel in the other grid, while dark gray surfaces show possible errors

tilings of the geometrical space by cubic voxels, each grid being positioned with respect to each other using this transform. One of the input images  $I_1$  being used as a geometrical reference, let us assume that its voxels are represented by elementary unit volumes of the canonical basis. The underlying idea is to build a set of vectors from the transform, which will generate the cubes that represents voxels in general position (voxels from  $I_2$ ).

In the case of brain imaging, a rigid transform is often sufficient to match images of cerebral structures from both data sets, since the brain is considered as a non-deformable solid. The rigid transform is initially composed of rotations and translations (6 parameters in 3D). A difference in spatial resolution implies a third part in the transform, based on the application of a scaling factor. In this case, let  $I_1$  be the image with the highest spatial resolution, and suppose that the registration operation aims at aligning  $I_2$  on  $I_1$ .

Let  $\mathbf{T}$  be the registration operator. The generating vectors of the base cube in general position are the images of canonical unit vectors by  $\mathbf{T}$ , and this cube has its origin on a point  $p \neq 0$  because of translation components in  $\mathbf{T}$  coming from the image registration ( $p = \mathbf{T} \cdot (0 \ 0 \ 0 \ 1)^t$  in homogeneous coordinates). Other cubes of the tiling are obtained by translation of this origin voxel. More details about the model building process may be found in (Montagner et al, 2005c).

Geometrical relations between the digital grids are then identified by processing spatial coefficients  $\rho$ , i.e. volumes of the polyhedra resulting from the intersection between cubic voxels in general position and unit cubes (Fig. 6.d).

The intersection volume between two given voxels  $V$  and  $v$  is computed using an efficient cube intersection algorithm (Reveilles, 2001). The processing cost is lower than the one obtained using a general convex polyhedra intersection algorithm, thanks to the use of cube symmetries and resulting analytical formulas. The algorithm runs through the 6 faces of both cubes, processing a polygonal boundary of the volume at each iteration. Let  $I$  be the polygon obtained as the intersection between the support plane  $P$  of the current cube square face  $F$  and the other cube (Fig. 6.a). Analytical formulas provide 3D coordinates of this intersection in a canonical space (Fig. 6.b), and the polygon is then brought back to its real position using the octahedral group of cube symmetries (Fig. 6.e). At this stage,  $I$  is possibly larger than the real polygonal face. It is therefore restricted to its common part with  $F$  (Fig. 6.c) using an adapted version of the O'Rourke's general polygon intersection algorithm (O'Rourke, 1998).

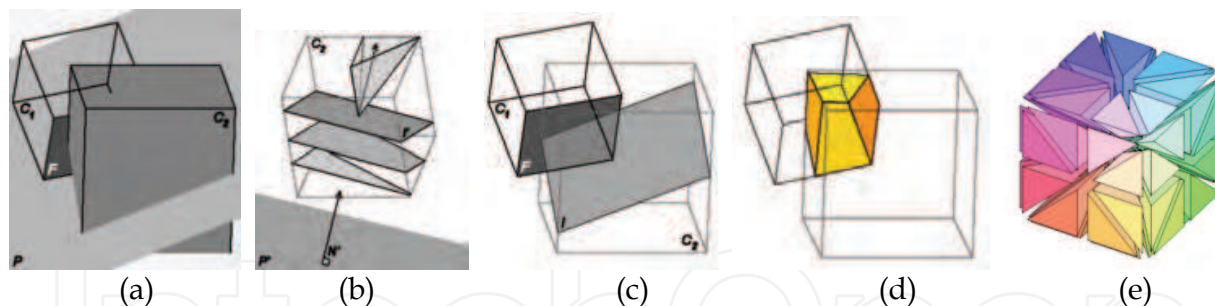


Fig. 6. a-c. Steps of the algorithm used to process the intersection polyhedron (d) between two cubic models of voxels  $C_1$  and  $C_2$ , using cube symmetries (e)

### 4.3 Final model aggregation stage: combination of numerical and geometrical information

If  $\rho$  is the result of the elementary fusion between basic elements  $v$  and  $V$  of the geometrical model, the final redistribution process can be expressed for general purpose as

$$\delta_{v,V} = \Delta\{\rho(v,V),g(V)\} \quad (2)$$

where  $\Delta\{\cdot,\cdot\}$  is the redistribution function, assigning to voxel  $v$  a part  $\delta_{v,V}$  of the information held by  $V$ , either in its direct form (initial image intensity in the case of the quantification process) or resulting from the image numerical modeling ( $g(\cdot)$  is a general information function). The final aggregation step then brings together the fusion operators from both domains to compute the result of the global fusion process. The elementary part of this result  $\varphi_{v,V}$ , for example in the spatial base of image  $I_1$  (e.g. at the highest spatial resolution) is processed as

$$\varphi_{v,V} = \varphi\{f(v),\delta_{v,V}\} = \varphi\{f(v),\rho(v,V),g(V)\} \quad (3)$$

where  $\varphi\{\cdot,\cdot\}$  is the aggregation operator, and  $f(\cdot)$  is another information function. Functions  $f(\cdot)$  and  $g(\cdot)$  represent information provided by image numerical models, or even stand for information derived from a first fusion stage in which spatial relations have no influence (case of the multistage use of the general fusion scheme).

Using the intersection volumes between voxels  $v$  and  $V$  as spatial coefficients  $\rho(v,V)$ , equation (2) thus simply becomes  $\delta_{v,V} = \rho(v,V) \cdot g(V)$ . Hence, the value assigned to voxel  $v$  is processed from the redistributed intensities of voxels  $V_i$  in a neighborhood of  $v$  as

$$\delta_v = \sum_{V_i \cap v} \rho(v,V_i)g(V_i) \quad (4)$$

where  $V_i \cap v$  refers to the set of voxels  $V_i$  having a non-null intersection with  $v$ . Formula (4) processes the value  $\delta_v$  associated with  $v$  as a combination of the information  $g(V_i)$  associated with surrounding voxels  $V_i$ , where the contribution of  $V_i$  is proportional to its common volume with  $v$ . As a matter of fact, this computation mode is very close to a linear interpolation of  $g(V_i)$ , in the case where  $v$  straddles several voxels  $V_i$ . But this process uses the maximum of information available in the image structure, thus minimizing the hypothesis required on the distribution of the physical phenomenon measured. When building image models, reference voxels  $v$  are moreover represented as unit volumes.

Spatial coefficients  $\rho(v, V)$  are thus numerical values ranging from 0 (no intersection between  $v$  and  $V$ ) to 1 (full intersection, i.e.  $v \subseteq V$ ), and  $\sum_{V_i \cap v} \rho(v, V_i) = 1$  for a given voxel  $v$ . The redistribution process is thus normalized so that each piece of information  $\delta_v$  naturally belongs to the same value range as the original numerical support of  $g(V)$ . In the case where  $v$  is fully included in  $V$  ( $\exists! V_i, V_i = V / V_i \cap v \neq \emptyset$ ), the information  $\delta_v = g(V)$  is kept unchanged since the whole unit volume stems from the intersection with a unique voxel  $V$ .

#### 4.4 Relations with data interpolation

As stated above, information redistribution expressed through equation (4) can be considered, from a computational point of view, as an interpolation of the numerical intensities from image  $I_2$ . But the interpolation is no longer uniform: the redistributed information is processed like in a nearest-neighbor interpolation when  $v \subseteq V$ , or is linearly interpolated with respect to intersection volumes when  $V$  intersects  $v$  boundaries. This adaptive way of processing minimizes the estimation error of the average activity in the set  $\{v_j / v_j \cap V \neq \emptyset\}$ , in comparison with a linear variation of  $\delta_{v_j}$  with respect to the distance to voxels  $V_i$ . Moreover, representing the spatial relation between input images through coefficients  $\rho$  establishes an accurate link between pieces of numerical information they hold without modifying them. This straightforward matching makes it possible to adapt numerical intensities stemming from image  $I_2$  to the content of image  $I_1$ , e.g. for measurement purpose. This second property will thus naturally find a direct application in the quantification of neuronal activity presented in section 5.3.

Finally, the redistribution principle is also characterized by two major methodological points: the nature of weighting factors in interpolation formulas, built from objective image spatial structure and relations, and the ability to introduce spatial coefficients into advanced aggregation models at the final aggregation step. Indeed, the general operation expressed by equation (2) can obviously be delayed, and split up into new parts of equation (3) so that coefficient  $\rho$ ,  $g(V)$  and  $f(v)$  are combined differently by the aggregation operator  $\phi$ .

## 5. Application to medical image analysis

### 5.1 Multispectral MR images fusion

The first application we propose is a 1 level/1 stage fusion scenario (Fig. 7.a), and concerns the fusion between several MR brain images stemming from different acquisition techniques. Images reflect the same type of knowledge (anatomical distribution of brain tissues), and provide complementary information with the use of different acquisition parameters. Numerous applications can benefit from the MR images fusion process, from abnormal tissue segmentation (tumors (Dou et al., 2006, Philipps et al., 1994), encephalitis, etc.) to the quantification of white matter, gray matter and cerebrospinal fluid volumes in normal (e.g. Wagner et al., 2006) or pathological people (e.g. Swayze et al., 2003).

The aim here is thus to extract  $C$  tissue classes from a set of  $n$  MR images. Following the theoretical framework proposed in this chapter, each MR image  $I_i$  first provides  $C$  distributions of possibility  $\pi_T^i$ , modeled as  $C$  fuzzy tissue maps. Given a tissue  $T$ , the corresponding  $C$  fuzzy maps have then to be fused using a fusion operator. Since the original MR images provide distinct but complementary information about the distribution

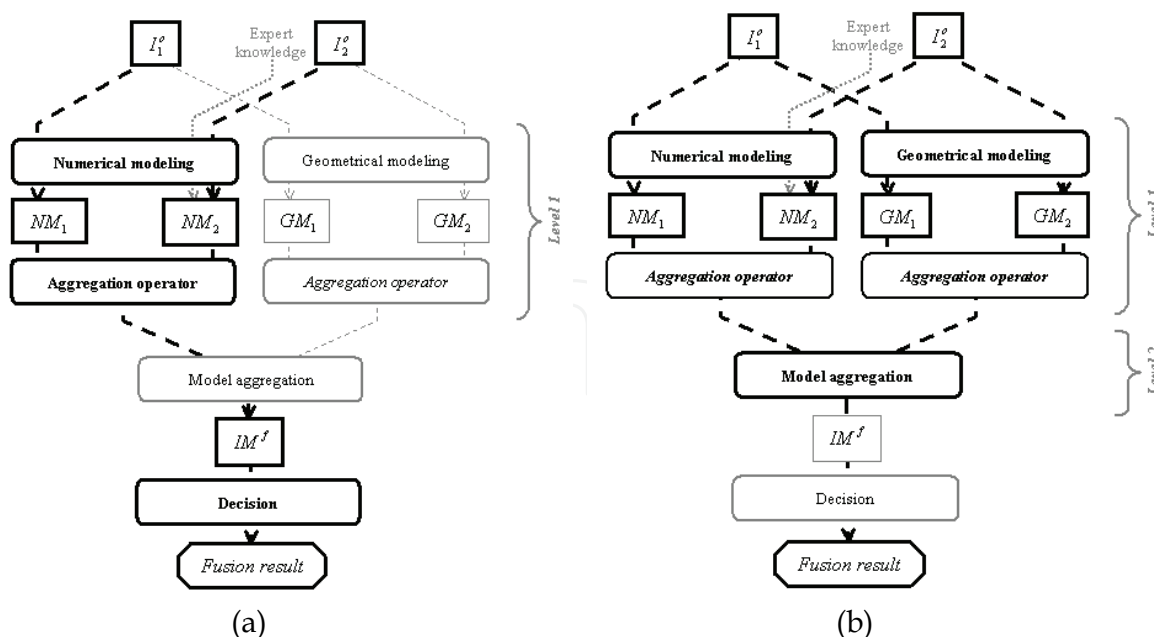


Fig. 7. Instantiation of the fusion scheme in the MR/MR fusion (a) and image synthesis examples (b). The decision step (defined in 2.1) concerns the production of segmented images in the first case, and is not applied in the second case (direct display of fusion result)

of  $T$  in the brain, the only areas of ambiguity may be due the transitions between  $T$  and neighboring tissues, or may be related to the pathological signature of  $T$  (e.g. a tumor imaged with a contrast agent may have a very significant hyper or hypo signal, not related to a pure anatomical acquisition). The fusion operator has thus not only to underline the redundancies between the  $\pi_T^i$  's, but also to shed light on possible areas of conflict between the distributions of possibility. We illustrate the construction of the fusion operator in the case  $n=2$ , and the extension to any  $n$  is trivial (Dubois & Prade, 1992). If both distributions of possibility  $\pi_T^1$  and  $\pi_T^2$  agree and are reliable, a renormalized T-norm is used to aggregate the information:

$$\pi_T = \min(\pi_T^1, \pi_T^2) / h \tag{5}$$

where  $h = 1 - \frac{(\sum |\pi_T^1(i) - \pi_T^2(i)|)}{N}$  measures the agreement between both distributions of possibility. On the contrary, if only one of the distributions is reliable, the operator has to be cautious and gradually reports the confidence on the union of the distributions, guided by  $(1-h)$ , an estimation of the conflict:

$$\pi_T = \min[\max(\pi_T^1, \pi_T^2), 1 - h] \tag{6}$$

In order to manage both situation, the final operator acts as

$$\pi_T = \max\left(\frac{\min(\pi_T^1, \pi_T^2)}{h}, \min[\max(\pi_T^1, \pi_T^2), 1 - h]\right) \tag{7}$$

This gives for each tissue  $T$  a fused distribution of possibility, and each voxel  $i$  is thus defined by  $C$  values  $(\pi_1(i) \dots \pi_C(i))$ . Since the aim of the fusion is to provide a volumetric quantification of brain tissues, the decision stage labels a voxel  $i$  as belonging to tissue  $\hat{T}(i)$  such as

$$\hat{T}(i) = \text{ArgMax}_T \{\pi_T(i)\} \quad (8)$$

As test data, we used simulated MR images generated with the online MRI Simulator at the McConnell Brain Imaging Centre (BrainWeb, <http://www.bic.mni.mcgill.ca/brainweb/>) in Montreal. The data sets are based on an anatomical model of a normal brain that results from registering and preprocessing of 27 scans from the same individual with subsequent semi-automated segmentation. In this data set the different tissue types are well-defined, both fuzzy and crisp tissue membership are allocated to each voxel. From this tissue labeled brain volume the MR simulation algorithm, using discrete-event simulation of the pulse sequences based on the Bloch equations, predicts signal intensities and image contrast in a way that is equivalent to data acquired with a real MR-scanner ( $T_1$ -weighted,  $T_2$ -weighted and Proton Density). Both sequence parameters and the effect of partial volume averaging, noise, and intensity non-uniformity (RF) are incorporated in the simulation results (Kwan et al., 1999). In order to obtain the true, i.e. reference volumes, the voxels labeled as gray, white matter and CSF in the discrete brain phantom (noise=0%, RF=0%) were counted. 20 additional simulated BrainWeb data sets that were used are each based on an anatomical model of an individual normal brain (for details see (Aubert-Broche et al., 2006)).

Figure 8 presents the results obtained for the fusion of several couples of images of the model. The  $T_1/T_2$  fusion provides a very accurate WM map, a CSF map very close to the one provided by the  $T_2$  image only, and a GM map suffering from several drawbacks (mainly a poor definition of some gray matter structures (basal ganglia)). The  $T_1/PD$  and the  $T_2/PD$  fusions exhibit a poorly informative CSF map, since both acquisitions suffer from a lack on information on the distribution of this tissue, especially in sub-arachnoid spaces. The other fused distributions are very close to those provided by BrainWeb.

Figure 9 shows the final segmentation map, obtained with the three types of fusion. Each segmented map was assessed with respect to the reference map provided by BrainWeb, both using an expert evaluation (a neurosurgeon visually assessed the accuracy of the segmented maps), and quantitative indexes:

- the confusion matrix  $M$ , giving for each tissues  $T$  and  $T'$  the number  $M_{TT'}$  of voxels being classified as  $T$  in the BrainWeb segmentation, and as  $T'$  in the computed segmented image;
- the Tanimoto indexes (TI) (Duda et al., 2001) computed from  $M$ , and allowing an accurate comparison between two segmentation results;
- for each tissue  $T$ , the relative errors (RE) in volumetric quantification between the computed map and the reference one.

Table 1 presents some of these results for the three types of fusion. Globally, best results were obtained with the  $T_1/T_2$  fusion process, those images being indeed very discriminant for brain tissue segmentation (Kiviniitty, 1984), but need a preliminary registration step.

Finally, Table 2 presents a comparison between the fusion method and three classical segmentation methods, either using a clustering algorithm on one image only, or a bidimensional histogram analysis in the  $(T_1, T_2)$  space. The best quantitative indexes were obtained using the fusion process, for all tissues.

	Réf	T <sub>1</sub> /T <sub>2</sub>		T <sub>1</sub> /PD		T <sub>2</sub> /PD				
	Vol (%)	TI	Vol (%)	RE <sub>T</sub> (%)	TI	Vol(%)	RE <sub>T</sub> (%)	TI	Vol(%)	RE <sub>T</sub> (%)
CSF	5,96	0.71	6.94	14.1	0.63	6.75	13.25	0.66	7,43	24.6
WM	23,5	0.82	22.72	3.32	0.85	23.13	1.57	0.75	24.14	2.72
GM	20,07	0.76	20.67	2.98	0.80	20.45	1.89	0.71	18.76	6.52

Table 1. Quantitative evaluation of the MR/MR fusion process

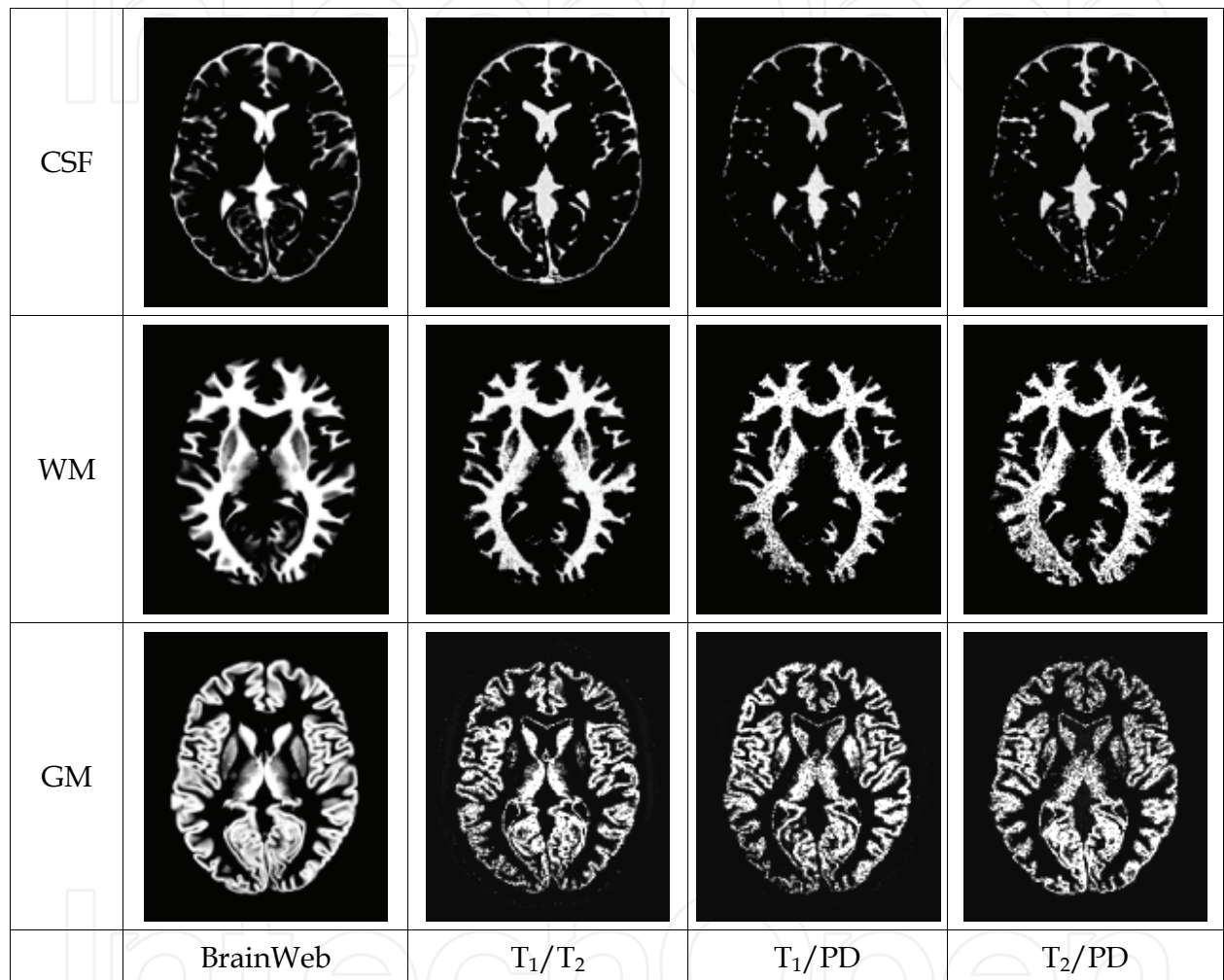


Fig. 8. Fused tissue maps

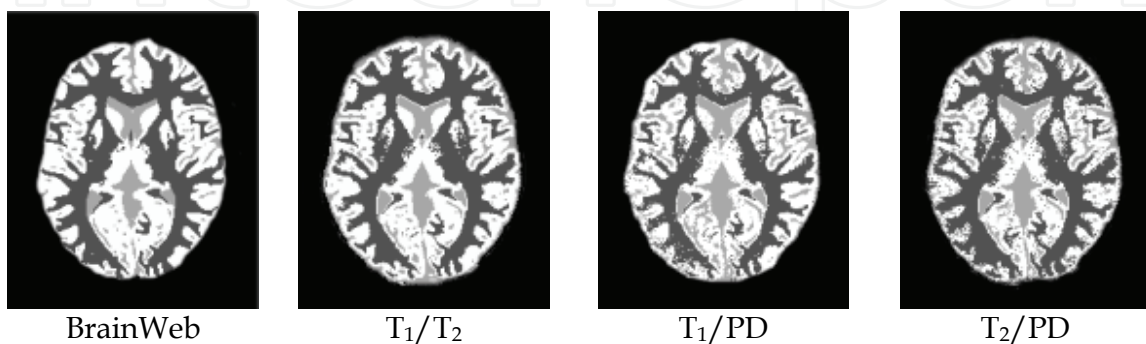


Fig. 9. Segmented images obtained from several fusion processes

	T <sub>1</sub> only		T <sub>2</sub> only		2D histo. analysis		T <sub>1</sub> /T <sub>2</sub> Fusion	
	TI	RE <sub>T</sub> (%)	TI	RE <sub>T</sub> (%)	TI	RE <sub>T</sub> (%)	TI	RE <sub>T</sub> (%)
CSF	0.63	14.2	0.79	13.6	0.67	15.98	0.77	14.1
GM	0.82	3.87	0.58	7.81	0.78	5.12	0.82	3.32
WM	0.76	3.14	0.65	5.45	0.76	3.05	0.76	2.98

Table 2. Comparison of segmentation results between the fusion method and classical algorithms

## 5.2 Image synthesis from multimodal information

This application of the general fusion scheme aims at accurately locating the functional information extracted from a SPECT image of the brain with respect to underlying anatomical structures. The difficulty of representing both complete pieces of information on the same image was pointed out in early studies on this subject (Hill, 1993), stating that the efficiency of displaying superimposed color layers decreases when the number of image features to show increases. Conversely, an advanced image fusion strategy, such as the one proposed in this chapter, can avoid spatial covering or frequency mixing by selecting features from each image that are relevant for diagnosis.

The image fusion is performed between an MR image, and either a brain perfusion or a neurotransmission SPECT image. The first functional imaging modality provides diagnostic information for brain pathologies where a visible reduction of blood supply is representative for the dead of neuronal cells in the related region of the brain, such as Alzheimer type dementia. The second one gives information about a specific neuronal activity, possibly responsible for pathologies such as Parkinson's disease and Parkinsonian syndromes (low level in target anatomical structures, mostly putamens and heads of caudate nuclei). In both cases, the difference in spatial resolution between MR and SPECT images requires a geometrical modeling of image spatial features, i.e. using the 2-level fusion capability of the fusion scheme (Fig. 7.b).

Referring to formula (2), the information function  $g(\cdot)$  is a direct reference to initial values associated with voxels  $V$  from image  $I_2 = I_f$  holding the functional information. Using the redistribution principle, the final model aggregation assigns to voxel  $v$  the redistributed intensity  $\delta_v$  processed from formula (4) with  $g(V) = I_f(V)$ , the original numerical value associated with  $V$  in the SPECT image. Formula (4) thus finally becomes

$$\delta_v = \sum_{V_i \cap v} \rho(v, V_i) I_f(V_i) \quad (9)$$

Let  $\pi_C(v)$  be the fuzzy membership degree of voxel  $v$  to the tissue class  $C$  (white matter, gray matter, and cerebrospinal fluid) from the numerical model of the MR image (computed as explained in section 3.2). An activity  $\mu_C$  is associated with each anatomical class, either from an arbitrary gray level adapted to the human visual perception to emphasize important information, or from a mean functional activity for class  $C$ . In each case,  $\mu_C$  may be considered as the second part of the numerical model representing image  $I_2$ . Anyway, the anatomical information is preserved in the global shape of brain tissue classes, and local variations of the functional activity within each class are injected, in addition to  $\mu_C$  in the proposed model, through the adapted form of equation (3):

$$\varphi_v = \frac{\sum_C \pi_C(v) \mu_C + \delta_v}{\sum_C \pi_C(v) + \sum_{V \cap v} \rho(v, V)} \quad (10)$$

where  $\delta_v$  is the redistributed functional activity mixing the geometrical information with original intensities from  $I_2 = I_f$  (first part of the numerical model for this image). The other part of the numerator stems from the aggregation of numerical models only,  $\mu_C$  (second part of numerical model for  $I_2$ ) being independent of any spatial context. Formula (10) is thus a good example of the introduction of spatial coefficients into advanced aggregation models detailed in section 4.4.

The image synthesis process has been applied to both brain perfusion SPECT ( $[^{99m}\text{Tc}]$ -ECD) and neurotransmission SPECT ( $[^{123}\text{I}]$ -FP-CIT) images, in the case of a patient suffering from a multiple system atrophy (MSA, Parkinsonism plus syndrome - Fig. 1). A single  $T_1$ -weighted MR data set is associated with perfusion and neurotransmission SPECT images, which were simultaneously acquired (El Fakhri et al., 2001). Both SPECT images and the pre-processed MR image are isotropic, with voxel sizes of 2.33 mm and 1.5 mm respectively. The quality of synthetic images (Fig. 10) was assessed by an expert, focusing on the following diagnosis elements: activity peaks and lacks, shape and position of anatomical structures. He answered the following questions for both the brain perfusion and the neurotransmission images:

1. Is the ability to locate functional activity in relation to anatomical structures really improved?
2. Are diagnosis elements clearly visible on the synthetic image?

For purpose of assisting the diagnosis task, the perfusion information (Fig. 10.a to d) has to be emphasized in the region of cerebral cortex (gray matter). The concentration level of the tracer within CSF structures is null. Variations are visible in the WM and mostly in the GM (activity ratio estimated to 1/4), corresponding to the above requirement. High activity levels in the cortical region are clearly visible, this effect being reinforced by the already high mean activity of this structure. Nevertheless, hypoperfusion zones are mostly visible in regions with low base activity, i.e. thanks to remaining diffused activity in the surrounding white matter.

In the case of the neurotransmission image (Fig. 10.e to h), the high activity bound in the striatum implies a decrease of visual contrast in the surrounding region. However, deducing the shape and position of anatomical structures remains possible thanks to the outlines of close tissue classes. Indeed the functional activity presents only low variations outside the striatum (CSF in the ventricular system and GM in the cortex). Likewise, edges of the putamens and caudate nuclei can also be deduced from areas with a low activity levels within the striatum itself (see Fig. 10.h). The synthesis process thus emphasizes the information brought by lacks of activity.

### 5.3 Quantification of functional activity using a multistage information fusion

The solution we propose for measuring brain activities in a SPECT image uses both the multilevel (management of multiresolution discrete data) and the multistage aspects of the fusion architecture (Fig. 11.a). This last point refers to modeling image activities as binary maps of subcortical brain structures used as measurement ROIs. This segmentation task is achieved as a second iteration of the fusion process (1 level/1 stage) with MR images and symbolic information as inputs (Fig. 11.b). We refer the reader to (Barra & Boire, 2001b) for a detailed description of this modeling stage.

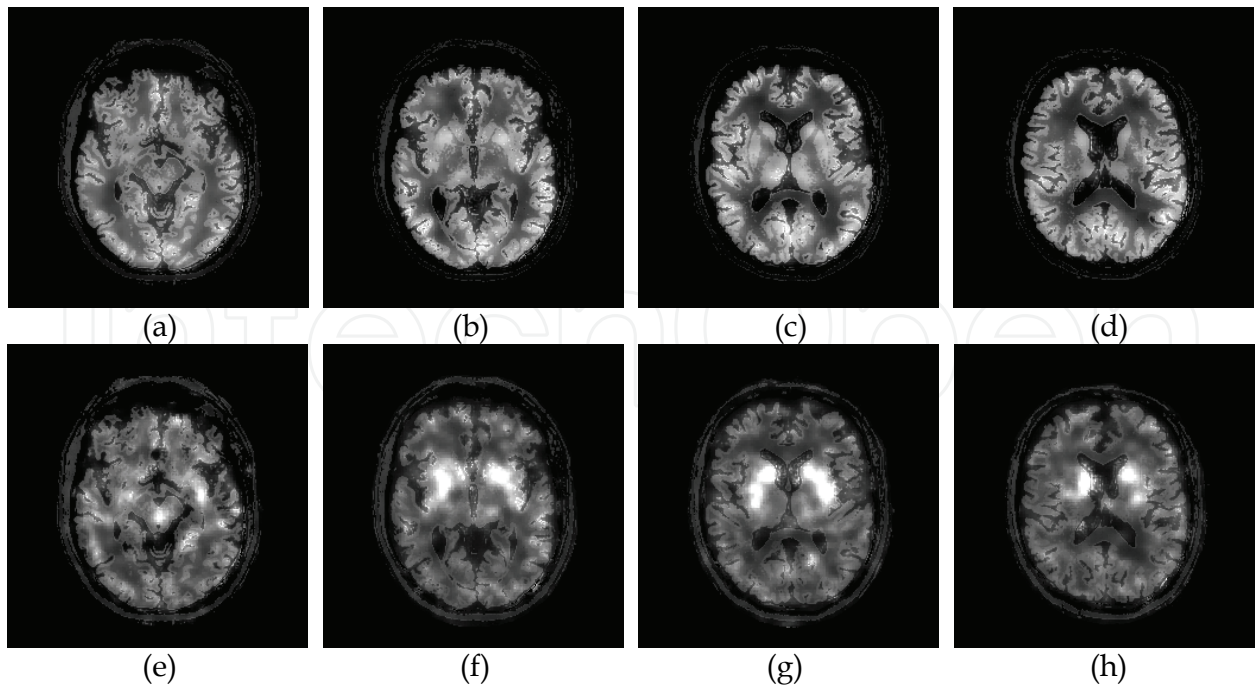


Fig. 10. Image synthesis from MR/perfusion fusion (a-d) and MR/neurotransmission fusion (e-h)

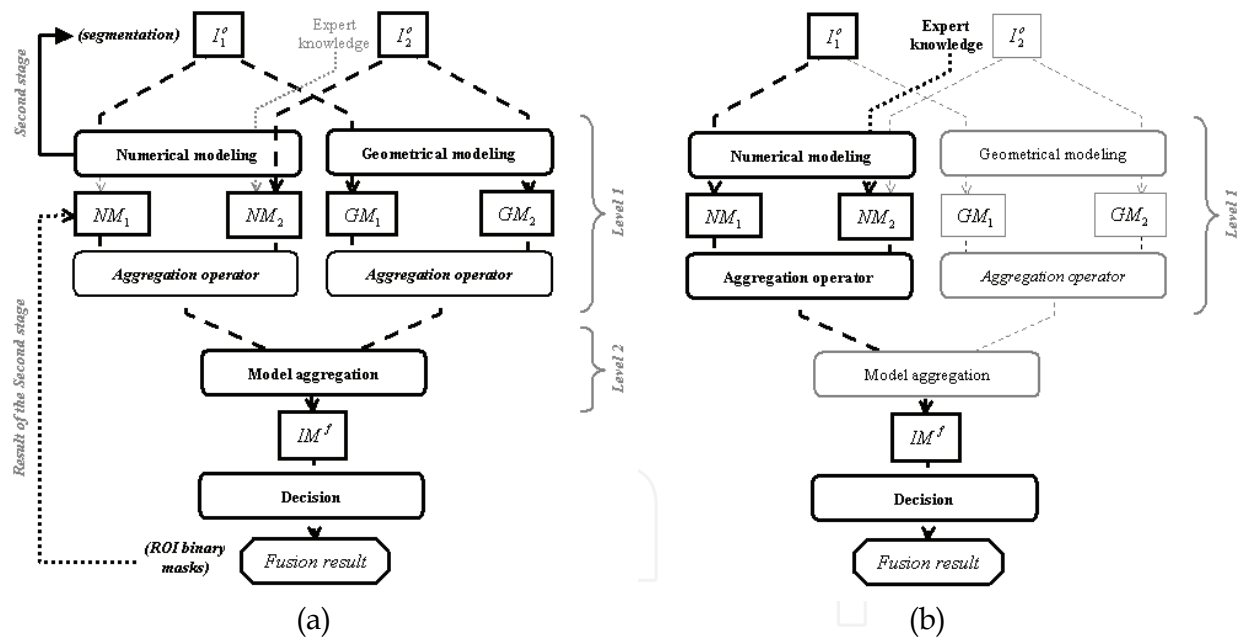


Fig. 11. Fusion scheme for the example of a brain activity quantification process (a); Original intensities from  $I_2^0$  (SPECT) are combined, through spatial coefficients, with ROIs Boolean models stemming from the second fusion stage (b); The decision in (a) may consist in classifying the whole SPECT exam according to the quantification index  $IM^f$

As in section 5.2 (and referring to equation (2)), the numerical model of a voxel  $V$  from the SPECT image is  $g(V) = I_f(V)$ , the original numerical value associated with  $V$ . Let  $S_a$  be this binary mask representing the brain structure of interest ('a' standing here for "anatomical"). The contribution of voxel  $v$  to the fusion result may thus be expressed as

$$\varphi_v = \sum_{V_i \cap v} \varphi_{v, V_i} = \sum_{V_i \cap v} S_a(v) \rho(v, V_i) I_f(V_i) = S_a(v) \sum_{V_i \cap v} \rho(v, V_i) I_f(V_i) = S_a(v) \delta_v \quad (11)$$

since formula (3) is also multiplicative with  $f(v) = S_a(v)$  (crisp membership) when using intersection volumes as spatial coefficients, and referring to equation (9). Consequently, the functional activity in out-of-structure anatomical voxels, in which the numerical expression of this activity is mostly due to the multiresolution partial volume effect (PVE), is naturally cancelled. The final result of the fusion process can be expressed as

$$\varphi = \frac{(\varphi_{S_t} - \varphi_{S_{ns}})}{\varphi_{S_{ns}}} \quad (12)$$

and is seen as an estimation of the radiotracer binding potential (Soret et al., 2003).  $\varphi_{S_t}$  is the global activity of the target anatomical structure (we use mean values), processed from the binary mask  $S_t$  through equations (11). In the same way, the quantity  $\varphi_{S_{ns}}$  is processed for a non-specific region of the brain (i.e. not influenced by the studied pathology).

The following tests have been carried out for a methodological assessment of the proposed quantification process. Since the method has been designed to overcome partial volume effects due to multiresolution, the assessment protocol aims at evaluating the accuracy of activity measurement from highly PVE-prone ROIs, in the context of several ratios of spatial resolutions between input images (this kind of PVE is mostly due to voxels from the functional image located at the external bound of the measurement region). The quantification has been performed on series of ROIs with a reference shape but different volumes (slice selection). Performances have been compared with the method considered as reference: registration of the MR image on the SPECT image.

The test dataset is made of a numerical phantom dedicated to the study of deep brain structures and dopamine neurotransmission phenomena involved in Parkinson's disease and Parkinsonian syndromes. It results from a Monte-Carlo simulation of the striatum-based neurotransmission (El Fakhri et al., 2001) using theoretical binding values in associated structures from a brain morphological phantom (Zubal et al., 1996). This phantom is also used as an anatomical reference for the data fusion process, and specially to build the image geometrical model. The functional image resulting from the simulation is initially aligned with the input data. A linear transform is applied to anatomical data to preserve the original functional information (including image rescaling by various factors, so that the ratio between voxel sizes is successively 1/2, 1/4 and 1/8). The initial measurement ROI is limited to right and left putamens. In simulated data, the tracer fixation ratio between putamens and the non specific (NS) reference region (here the occipital cortex) corresponds to a healthy case.

Table 3 shows the results obtained when quantifying the phantom activity within regions described above. Results are assessed in terms of relative error  $|\varphi - \varphi_{ref}| / \varphi_{ref}$ , where  $\varphi$  is the estimated binding potential (BP) processed through equation (12) with  $\varphi_{S_t}$  relative to the truncated putamens and  $\varphi_{S_{ns}}$  standing for the non-specific occipital cortex region.  $\varphi_{ref}$  refers to the same quantity, processed from the *a priori* model activities. Error values are averaged from quantities measured after applying linear transforms with 5 sets of parameters (rotation angles and translation vectors).

The quantification error is always lower for the redistribution method. The maximum difference is obtained for a resolution ratio of 1/4, due to the value quantified within the non specific region, that has a high influence on the BP estimated (see equation (12)). Conversely, the irregular and thin shape of this structure allow results to be quite constant (between ratios

1/2 and 1/4) using the MR registration method. The higher the resolution ratio, the more constant the size of the interpolated ROI, because of the effects of thresholding mask coefficients. The minimum error always corresponds to the largest measurement ROI (close to initial volume), and the maximum value to the thinnest one, except in the case of redistributions with a ratio of 1/8, due to the influence of the NS region again.

		Resol. ratio 1/2		Resol. ratio 1/4		Resol. ratio 1/8	
		Error (%)	Volume	Error (%)	Volume	Error (%)	Volume
MR image regist.	Min.	20.4	9909	24.8	9625	44.6	8859
	Max.	34.0	1341	24.9	9710	44.6	8859
Redistribution	Min.	11.8	9923	2.9	9918	24.16	1961
	Max.	24.7	1980	8.6	1691	31.2	9920

Table 3. Minimum and maximum relative quantification errors (depending on the actual volume of the measurement ROI, also indicated in cm<sup>3</sup> for comparison with the volume of the original putamen structure = 10<sup>4</sup> cm<sup>3</sup>, that provided the quantitative reference value)

## 6. Conclusion

The collection of anatomical and functional images, as well as the expert knowledge and habits play nowadays in clinical routine an important role for the study of a given pathology. The clinician merges and aggregates all this complementary, redundant and sometimes conflicting information to provide a better diagnosis. We proposed in this chapter a theoretical framework mimicking this aggregation process, based on the use of fuzzy logic modeling, fusion operators, and we enrich this classical fusion process with the introduction of spatial information modeling. This allows the information to be preserved until the final fusion step, and gives the opportunity to introduce the original image information into complex fusion operators. We provide the clinician with several outputs, from segmented images to quantitative indexes or synthesis images, and we think our process to be generic enough to allow the introduction of other information sources.

The multilevel information fusion is applied to three clinical applications, involving anatomical and functional images, and also geometrical and structural information. Results prove the efficiency of the approach, and shed light on several potential new applications not only in brain imaging, but also in the multimodal study of other organ, or even to other branches where several images, with several geometrical properties, are used, registered and merged.

## 7. References

- Aguilar, M. & New, J.R (2002). Fusion of multi-modality volumetric medical imagery, *Proceedings of the Fifth International Conference on Information Fusion*, 2:1206-1212
- Aubert-Broche, B.; Collins, D. & Evans, A. (2006). A new improved version of the realistic digital brain phantom. *Neuroimage*, 32:138-145.
- Barra, V., & Boire, J. Y. (2000a), Tissue Characterization on MR Images by a possibilistic Clustering on a 3D Wavelet Representation, *Journal of Magnetic Resonance Imaging*, 11:267-278.
- Barra, V., & Boire, J. Y. (2000b). Aggregation of anatomical and functional Information by a MR/SPECT fusion process: Application to neurodegenerative Pathologies – *Proceedings of the Sixth Annual Meeting of the Organization for Human Brain Mapping*, San Antonio. *NeuroImage* 11.

- Barra, V. & Boire, J.Y (2001a): A general framework for the fusion of anatomical and functional medical images. *NeuroImage* 13:410-424.
- Barra, V. & Boire, J.Y (2001b): Automatic Segmentation of subcortical brain Structures in MR Images using Information Fusion, *IEEE Transactions on Medical Imaging*, 20:549-58.
- Bloch, I. (1996). Information combination operators for data fusion: a comparative review with classification. *IEEE Transactions on Systems, Man, and Cybernetics* 1:52-67.
- Bloch I. & Maître H. (1997). Fusion of Image Information under Imprecision. In B. Bouchon-Meunier, editor, *Aggregation and Fusion Of Imperfect Information*, Series Studies in Fuzziness. Physica Verlag, Springer.
- Bloch, I., Géraud, T. & Maître, H. (2003). Representation and fusion of heterogeneous fuzzy information in the 3D space for model-based structural recognition - Application to 3D brain imaging. *Artificial Intelligence* 148:141-175.
- Boussion N., Hatt M., Lamare F., Bizais Y., Turzo A., Cheze-Le Rest C. & Visvikis D. (2006). multiresolution image based approach for correction of partial volume effects in emission tomography, *Physics in Medicine and Biology*, 51:1857-1876.
- Catafau A. M. (2001). Brain SPECT of dopaminergic neurotransmission: a new tool with proved clinical impact, *Nuclear Medicine Communications*, 22:1059-1060.
- Colin, A. & Boire, J.Y (1999). MRI-SPECT fusion for the synthesis of high resolution 3D functional brain images: a preliminary study. *Computer Methods and Programs in Biomedicine* 60: 107-116.
- Dasarathy, B. V. (1997). Sensor fusion potential exploitation-innovative architectures and illustrative applications. *Proceeding of the IEEE*, 85(1):24-38.
- Dubois, D. & Prade, H. (1992). Combination of Information in the Framework of Possibility Theory, In: *Data Fusion in Robotics and Machine Intelligence*, M. Al Abidi et al. Eds, New York Academic.
- Dubois D. & Prade H. (1994). Possibility theory and data fusion in poorly informed environments. *Control Engineering Practice*, 2:811-823.
- Dubois D. & Prade H. (2004). Possibilistic logic: a retrospective and prospective view, *Fuzzy Sets and Systems* 144:2-23.
- Duda, R., Hart, P. & Stok, D. (2001). *Pattern classification*, New York: John Wiley & Sons.
- Dou, W.; Ruan, S.; Chen, Y.; Bloyet, D. & Constant, JM. (2006). A framework of fuzzy information fusion for the segmentation of brain tumor tissues on MR images, *Image and Vision Computing*, 25(2):164-171.
- El Fakhri G., Moore S.C., Maksud P., Aurengo A. & Foley Kijewski M. (2001). Absolute Activity Quantitation in Simultaneous 123I/99mTc Brain SPECT, *Journal of Nuclear Medicine*, 42:300-308.
- Hill D. (1993). Combination of 3D medical images from multiple modalities, *Thesis, University of London, London, England*.
- Hudson H. & Larkin R. (1994). Accelerate image reconstruction using ordered subsets of projection data, *IEEE Transactions on Medical Imaging* 13: 601-609.
- Julin, P., Lindqvist, J., Svensson, L., Slomka, P., & Wahlund, L. (1997). MRI-guided SPECT measurements of medial temporal lobe blood flow in Alzheimer's disease. *Journal of Nuclear Medicine*. 38:914-919.
- Kiviniitty, K. (1984). NMR relaxation Times in NMR Imaging, *Annals of Clinical Research*, 40 4-6.
- Krishnapuram R. & Keller J.A. (1993), A Possibilistic Approach to Clustering, *IEEE Transactions on Fuzzy Systems*, 1:98-110.
- Krishnapuram R. & Keller J.A. (1996), The Possibilistic C-Means Algorithm: Insights and Recommendations, *IEEE transactions on Fuzzy Systems*, 4:385-393.

- Kwan, R.; Evans, A. & Pike, G. (1999). MRI simulation-based evaluation of image processing and classification methods, *IEEE Transactions on Medical Imaging*, 18:1085-1097.
- Lennon, M.; Mouchot, M.C.; Mercier, G.; Solaiman, B. & Hubert-Moy, L. (2000) Segmentation of airborne hyperspectral images by integrating multi-level data fusion, *Proceedings of the Third International Conference on Information Fusion*, vol.2, 10-13 July 2000.
- Matsopoulos, G.K., Marshall, S. & Brunt, J.N.H. (1994). Multiresolution morphological fusion of MR and CT images of the human brain. *Proceedings of the IEEE Vision, Image and Signal Processing Conference* 141:137-142.
- Montagner J., Barra V. & Boire J.-Y. (2005a), Synthesis of a functional information with anatomical landmarks by multiresolution fusion of brain images, in *Proceedings of the 27th IEEE Engineering in Medicine and Biology Society Conference*, Shanghai, China.
- Montagner, J., Barra, V., Reveillès, J.P. & Boire, J.Y. (2005b). Multiresolution images fusion for the quantification of neuronal activity: a discrete approach. *Proceedings of the 3rd IASTED International Conference on Biomedical Engineering*, Innsbruck-Austria 1-6.
- Montagner, J., Barra, V. & Boire, J.Y. (2005c). Modeling of a multimodal image aggregation process using discrete geometry. *Proceedings of the 1st Open International Conference on Modeling and Simulation*, Clermont Ferrand-France 431-439.
- O'Rourke J. (1998). Computational geometry in C, 2nd ed. New-York, USA: Cambridge University Press.
- Pajares, G. & De La Cruz, J.M. (2004). A wavelet-based image fusion tutorial, *Pattern Recognition*, 37:1855-1872.
- Philipps, W.; Velthuizen, R.; Phuphanich, S.; Hall, L.; Clarke L. & Silbiger M. (1995). Application of Fuzzy C-Means Algorithm Segmentation Technique for Tissue Differentiation in MR Images of a Hemorrhagic Glioblastoma Multiforme, *Magnetic Resonance Imaging*, 13(4):277-290.
- Reveillès J.-P. (2001). The geometry of the intersection of voxels spaces, *Electronic Notes in Theoretical Computer Science*, 46:285-308.
- Rousset O. G., Ma Y., & Evans A. C. (1998). Correction for partial volume effects in PET: principle and validation. *Journal of Nuclear Medicine*, 39:904-911.
- Shafer, G. (1976). A mathematical theory of evidence. Princeton University Press, Princeton.
- Soret M., Malick-Koulibaly P., J.Darcourt, Hapdey S. & Buvat I., (2003). Quantitative accuracy of dopaminergic neurotransmission imaging with 123I SPECT, *Journal of Nuclear Medicine*, 44:1184-1193.
- Swayze, V.; Andersen, A.; Andreasen, N.; Arndt, S.; Sato, Y. & Ziebell, S. (2003). Brain tissue volume segmentation in patients with anorexia nervosa before and after weight normalization, *International Journal of Eating Disorders*, 33(1):33-44.
- Wagner, A.; Greer, P.; Bailera, U.; Frank, G.; Henry, S.; Putnam, K.; Meltzer, C.; Ziolkowski, S.; Hoge, J.; McConaha, C. & Kay, W. (2006). Normal Brain Tissue Volumes after Long-Term Recovery in Anorexia and Bulimia Nervosa, *Biological Psychiatry*, 59:291-293.
- Wald L. (2002) Data fusion : definitions and architectures - Fusion of images of different spatial resolutions, Les Presses de l'Ecole des Mines (pub.), Paris, France.
- Wang Y, Freedman M.T., Xuan J., Zheng Q., & Mun S.K. (1998). Multimodality medical image fusion: Probabilistic quantification, segmentation, and registration, *Proceedings of SPIE: Image display*, San Diego CA, 22-24, 3335:239-249.
- Zadeh, L.A. (1978). Fuzzy sets as a basis for a theory of possibility. *Information and Control*, 8:338-353.
- Zubal, I. G., Harrell, C. R., Smith, E. O., Smith, A. L. & Krischlunas, P. (1996). High resolution, MRI-based, segmented, computerized head phantom. *Proceedings of the 6th International Radiopharmaceutical Dosimetry Symposium*, Gatlinburg, 319-324



## **Sensor and Data Fusion**

Edited by Nada Milisavljevic

ISBN 978-3-902613-52-3

Hard cover, 436 pages

**Publisher** I-Tech Education and Publishing

**Published online** 01, February, 2009

**Published in print edition** February, 2009

Data fusion is a research area that is growing rapidly due to the fact that it provides means for combining pieces of information coming from different sources/sensors, resulting in ameliorated overall system performance (improved decision making, increased detection capabilities, diminished number of false alarms, improved reliability in various situations at hand) with respect to separate sensors/sources. Different data fusion methods have been developed in order to optimize the overall system output in a variety of applications for which data fusion might be useful: security (humanitarian, military), medical diagnosis, environmental monitoring, remote sensing, robotics, etc.

### **How to reference**

In order to correctly reference this scholarly work, feel free to copy and paste the following:

Julien Montagner and Vincent Barra (2009). Multilevel Information Fusion: A Mixed Fuzzy Logic/Geometrical Approach with Applications in Brain Image Processing, Sensor and Data Fusion, Nada Milisavljevic (Ed.), ISBN: 978-3-902613-52-3, InTech, Available from:

[http://www.intechopen.com/books/sensor\\_and\\_data\\_fusion/multilevel\\_information\\_fusion\\_\\_a\\_mixed\\_fuzzy\\_logic\\_geometrical\\_approach\\_with\\_applications\\_in\\_brain\\_i](http://www.intechopen.com/books/sensor_and_data_fusion/multilevel_information_fusion__a_mixed_fuzzy_logic_geometrical_approach_with_applications_in_brain_i)

**INTECH**  
open science | open minds

### **InTech Europe**

University Campus STeP Ri  
Slavka Krautzeka 83/A  
51000 Rijeka, Croatia  
Phone: +385 (51) 770 447  
Fax: +385 (51) 686 166  
[www.intechopen.com](http://www.intechopen.com)

### **InTech China**

Unit 405, Office Block, Hotel Equatorial Shanghai  
No.65, Yan An Road (West), Shanghai, 200040, China  
中国上海市延安西路65号上海国际贵都大饭店办公楼405单元  
Phone: +86-21-62489820  
Fax: +86-21-62489821

© 2009 The Author(s). Licensee IntechOpen. This chapter is distributed under the terms of the [Creative Commons Attribution-NonCommercial-ShareAlike-3.0 License](#), which permits use, distribution and reproduction for non-commercial purposes, provided the original is properly cited and derivative works building on this content are distributed under the same license.

IntechOpen

IntechOpen